SUPPLEMENTAL METHODS

EXPOSURE DATING

To sample the shoreline we selected a site about 280 m west of the nearest inselberg (Jebel Hawaja; Figure 1c) to reduce the possibility of slope wash reaching the sample site. Aerial images show slope wash halos around the inselbergs and a post-depositional alluvial fan 2 m thick flanking the inselberg and extending over the adjacent shoreline to at least 100 m. A 3 m trench (Section S2 of Williams et al., 2010) was excavated using a bulldozer and 6 samples were collected at 0.5 m intervals down the pit wall (Table DR1). Field observations and particle size analysis (Figure 2a-b) show a decrease in gravel content and an increase in sand from the base upwards, consistent with lake retreat, a decrease in wave energy and final deposition of a sandy beach at the site. A well developed soil has subsequently formed on top of the shoreline sediment.

The granite was crushed and a coarse quartz concentrate was prepared using heavy liquids and magnetic separation. Only the coarse sand (>0.5 cm) and gravel fraction of the shoreline sediment was used for ^{10}Be analysis. We purified quartz and extracted ^{10}Be using standard methods (Barrows et al., 2001). The surface sample was run in duplicate. Isotopic ratios (^{10}Be/Be) were measured by accelerator mass spectrometry on the 14UD accelerator at the Australian National University.

To investigate the potential for sequential deposition of the shoreline and to quantify inheritance of cosmogenic nuclides in the sand and gravel, we used a profile dating approach. Prolonged exposure of a sediment column to cosmic rays produces a characteristic cosmogenic nuclide depth profile that is a function of the production rate of the nuclide, sediment density, the accumulation or erosion rate of the sediment, and inherited nuclides in the sediment from previous exposure at the sediment source. Ideal conditions for exposure dating a profile are rapid deposition, an absence of post-depositional accumulation or erosion of the surface, and rapid erosion rates at the sediment source, which delivers a minimal inherited nuclide component. The setting of the Jebelein shoreline satisfies these suitability criteria. The ridge represents a high-energy depositional environment and therefore was deposited in a brief period of time. Second, there is no geomorphic evidence for widespread erosion of the surface in the form of gullying. Third, there appears to have been limited post-depositional accumulation of sediment on the surface. However, inheritance is likely to be significant because weathering rates are low on inselbergs in desert environments (e.g., Bierman and Caffee (2002)).

Cosmogenic nuclide production rates are a topic of active research and currently no consensus has emerged as to a ^{10}Be production rate and a single scaling scheme that is globally applicable. The CRONUS calibration data set gives a ^{10}Be production rate by

spallation of 4.49 ± 0.39 atom $g^{-1}a^{-1}$ at high latitude and sea level using the Stone (2000) scaling scheme (Balco et al., 2008). However, recent calibrations indicate that this rate is too high by at least 10% (Balco et al., 2009; Fenton et al., 2011; Kaplan et al., 2011; Putnam et al., 2010). In the absence of a regional production rate calibration, we used the North American regional production rate of Balco et al. (2009) which is at a similar elevation (<500 m) and within uncertainties is the same as another recent Northern hemisphere calibration (Fenton et al., 2011). It also has a longer calibration exposure age incorporating more geomagnetic variability. To scale the production rates we use the scaling scheme of (Lifton et al., 2005). Barrows et al. (2013) have shown that the Lifton et al. (2005) scheme produced the best match between ^{10}Be and radiocarbon dates in New Zealand. The calculated ^{10}Be concentrations, ages and weathering rates are given in Supplemental Table DR2.

To determine the exposure age for the profile, we updated the coefficients of the equations used in Granger and Smith (2000) for the ^{10}Be production rate of Balco et al. (2009) from that of Stone (2000). Maximum likely inheritance on the gravel was determined by processing three samples from the top of the adjacent Jebel Hawaja. The morphology of the inselbergs at Jebelein, including exfoliation and solution pits, indicates a low long-term weathering rate.

The uppermost part of the section appears to be reworked. OSL dating of fine sand in the surface soil at a depth of 56 cm yielded an apparent age of 3.0-3.1 ka (Williams et al., 2010). Fine sand from 106 cm showed very high dispersion and had equivalent dose values at about 1.5 Gy and 120 Gy, corresponding to ages between 2.0 ka and 158 ka. Additionally a portable dolerite murhakah (lower grinding stone) was found within the soil after excavation, but from an unknown depth. The age of this grindstone is difficult to determine because their use extends from the upper Palaeolithic through to the recent. Dozens of grinding holes and thick camp site hearth deposits of charcoal and broken bone line the edges of nearby inselbergs adjacent to the Nile River and indicate an important site of Neolithic habitation during a time when grassland was more widespread, probably before 4,500 ^{14}C yr BP. We therefore consider it likely that the grindstone was incorporated into the profile during the mid Holocene and therefore the upper part of the sediment profile was probably reworked at this time. It is also possible that some slope wash from the inselberg has reached the site and lowered the mean ^{10}Be concentration of the surface sediment. For these reasons we chose to analyse the coarse sand and gravel which has a much lower potential for translocation both up and down the profile. Our logging showed original bedding of the coarse clasts below the soil (Fig. 2a).

We used the CRONUS online calculator (Balco et al. 2008) to calculate the ^{10}Be production rate at the site. The exposure age (together with inheritance) was calculated from a least squares fit of a curve that is a sum of exponentials representing spallation, slow muon capture and fast muons (Granger and Smith, 2000). Because the relative errors are similar on each sample, we did not weight the fit.

The density of the sediment varies through the profile and so it was not possible to determine an integrated mean density for use in the calculations. The density of sand and gravel mixtures ranges from 1.6-2.1 g/cm^3, so we chose a density of 1.9 g/cm^3. Variations of

0.1 g/cm^3 in density change the exposure age by ~2 %. A density of 2.7 g/cm^3 was used for the granite samples. The quoted uncertainties are 68% confidence limits incorporating all known sources of measurement error, and include fully propagated production rate errors.

OPTICALLY STIMULATED LUMINESCENCE

Seven samples were collected for optically stimulated luminescence (OSL) dating from channel sands and overlying sediments, and one sample was collected from the modern White Nile to assess the extent to which the OSL signal is reset at deposition in this environment. Samples were collected by inserting an opaque tube into the sediment. This was then sealed at both ends and wrapped in black plastic. In the laboratory the material from both ends of the tube, which would have been exposed to light, was scraped out and used for environmental dose rate measurements.

Samples were processed either at Aberystwyth University or at the University of Adelaide. The comparability of the two sets of analysis has previously been demonstrated (Macklin et al., 2013). Samples were prepared using similar procedures in both laboratories. Samples were initially treated with hydrochloric acid to digest carbonates and hydrogen peroxide to remove any small amounts of organic material. Grains in the ranges 180–212 μm (Aberystwyth) and 125-180 μm (Adelaide) were selected by dry sieving. Solutions of sodium polytungstate were used to isolate grains with a density between 2.62 and 2.70 g/cm^3. Grains were etched for 40 minutes in 40% hydrofluoric acid to remove feldspar and other non-quartz material and to remove the outer 9 μm of the quartz grains. This eliminates the effect of alpha particle contribution to the irradiation of the grains. The material was then re-sieved to remove any remaining feldspar grains. All the laboratory procedures were carried out in subdued red light.

In Adelaide, uranium (U), thorium (Th) and potassium (K) concentrations were measured by Genalysis Laboratories, Perth, using Inductively Coupled Plasma Mass Spectroscopy (ICPMS) for U and Th, and Inductively Coupled Plasma Atomic Emission Spectrometry (ICPAES) for K. U and Th concentrations were also measured by thick source alpha counting (TSAC) in the Adelaide laboratory, and K concentrations by CSIRO laboratories, Adelaide, using X-ray fluorescence spectroscopy (XRS). The cosmic ray contribution was obtained using the relationship between cosmic ray penetration, depth and latitude determined by Prescott and Hutton (1994). The radionuclide concentrations obtained by the various methods were averaged, and the dose rate to be used in the age calculation, as well as the beta and gamma contributions to this dose rate, was determined using the AGE program of Grün (2009).

In Aberystwyth, beta dose rate was determined using a Risø beta counter (Bøtter-Jensen and Mejdahl, 1988), and the concentration of U, Th and K in the samples was determined using geochemical methods. For each sample, a finely milled sub-sample was fused using a sodium metaborate flux and put into solution. The resulting solutions were analysed using ICP-OES to determine the concentration of K and ICP-MS to determine the concentration of U and Th. The conversion factors of Adamiec and Aitken (1998) were then used to calculate the gamma dose rate. The cosmic ray contribution was obtained using the

relationship between cosmic ray penetration, depth and latitude determined by Prescott and Hutton (1994). Water content of the material as received was measured by weighing, drying overnight at 180ºC, and re-weighing. A value of 5 ± 2% was used as the best estimate of the water content during the period of burial for all samples except the sample from the modern White Nile where a value of 10 ± 5% was used (Note: an increase of 1% in the water content causes an increase of approximately 1% in the measured age of the sample). The results of these measurements are given in Table DR3, and the calculated dose rates are given in Table DR4.

Luminescence measurements for sample S10/5-2 were carried out at the University of Adelaide, and the other six samples including the surface sample were measured at the Aberystwyth Luminescence Research Laboratory (ALRL) at Aberystwyth University.

Luminescence measurements

In Aberystwyth luminescence measurements were made on aliquots containing ~500 grains of quartz between 180-212 µm in diameter, whilst for the sample measured in Adelaide aliquots with 50 to 100 grains (125-180µm diameter) were used. A Risø TL/OSL reader model TL-DA-15 was used for measurements in Aberystwyth, and a TL-DA-20 in Adelaide. In both laboratories blue LEDs (470Δ20 nm) were used for optical stimulation, and the resulting OSL was detected using EMI 9635QA photomultipliers fitted with Hoya U-340 filters. The resulting OSL signals showed a rapid initial decrease in intensity (Fig. DR1a) as would be expected from samples where the OSL signal is dominated by the fast component. The SAR method was used (Murray and Wintle, 2000), and typically 6 regeneration doses plus a zero dose point to test for recuperation, a repeat of the first dose to test for acceptable recycling and a second repeat of the first dose followed by exposure to infra-red radiation to test for the absence of feldspars (IR depletion test, Duller (2003)) were used to characterise the dose response curve and calculate the equivalent dose (D_e) for each aliquot (Fig. DR1b). Uncertainties on individual D_e values were determined using the approach outlined in Duller (2007) which incorporates the uncertainty due to counting statistics on each individual OSL decay curve, the uncertainty in the curve fitting procedure, and also a 1.5% uncertainty associated with the Risø instruments used for these measurements. Twenty-four replicate measurements of D_e were made for each sample. Data was screened using standard acceptance criteria, including (1) a recycling ratio within 10% of unity (15% for the sample analysed in Adelaide), (2) an IR depletion ratio (Duller, 2003) within 10% of unity (15% in Adelaide), (3) a net OSL signal from the test dose that is at least three times larger than the standard deviation of the background, (4) a dose response curve that increases monotonically, (5) recuperation, as measured for the zero dose point, that is less than 15% of the natural signal, and (6) a natural signal (and associated uncertainty) that intersects with the dose response curve. This screening removed very few aliquots, with between 21 and 24 aliquots passing all of these criteria.

The modern sample from the White Nile (S11/WN1) gave an age of 0 ± 21 years, demonstrating that quartz is very effectively reset by exposure to daylight at the time of deposition in this environment. One of the limitations of luminescence dating is the impact of saturation of the OSL signal at high doses. The form of the dose response curve (Fig. DR1b)

is either a single saturating exponential, or the sum of two saturating exponential functions. As the radiation dose to which a sample is exposed increases, the rate of growth of the OSL signal decreases, until at some point there is negligible growth. Beyond this point it is not possible to resolve samples of different age. A number of the samples in this study have large D_e values (> 100 Gy, Table DR4), but no more than 2 aliquots from 24 measured for each sample failed because the OSL signal was saturated. However, one feature of the samples with a high D_e (> 100 Gy) is that they tend to have dose distributions (Fig. DR1c) with overdispersion values (25-30%) slightly higher than is normally encountered in younger samples, and this is thought to result from curvature of the dose response curve. There is no evidence that this overdispersion is related to incomplete resetting of the luminescence signal at deposition, and the age of 0 ± 21 years for the modern sample supports this. Therefore, the D_e values for each sample were combined using the central age model (CAM) to derive a final D_e value for age calculation. The equivalent doses, dose rates and ages for all the luminescence samples are summarised in Table DR4.

LAKE RECONSTRUCTION

The SRTM90m digital elevation model (DEM) released by NASA has a 3 arc second horizontal resolution and a ~5 m vertical precision in this region, and was used to map the White Nile River valley in ArcGIS (Figs. 1A, 1B). Shorelines are most prominent north of 11° N in the Nile valley (Williams et al., 2003) and we mapped these directly from the DEM and CNES/SPOT imagery (Fig 1C) using the break in slope. The lake margin is indistinct in the south because of the low gradient of the Nile valley and we conservatively estimated the margin using the break in slope of the 400 m contour, the last contour to match the height of prominent shoreline features. Slope gradients are similar on both sides of the White Nile in the south, but significant shoreline features are present only on the eastern shore. The absence of significant shorelines in the west is due to three main factors: the most likely dominant wave direction is from the south west, destruction by the Khor Abu Habl alluvial fan, and encroachment of linear dune fields. In the region of the Khor Abu Habl fan and linear dune fields of the western margin we followed contours reflecting the height of shoreline features on the opposite side of the lake and this is a conservative estimate for the lake width. North of 13.5° N we graded the lake margin to the 390 m contour to match the entry points of the Blue Nile palaeochannels. The height of the shoreline drops by ~10 m over a distance of 650 km, indicating a gradient of ~ 1: 65,000, about 70% of the modern river gradient and reflecting incomplete damming of the lake. The area and volume of the palaeolake were calculated in ArcGIS by using the polygon volume (3D analyst) function. First, a triangulated irregular networks (TIN) surface was created by selecting parameters that would best conform to the 90 m surface DEM. The lake was then subdivided into three polygons reflecting where the shorelines matched the 400, 395 and 390 m contours, in order to obtain the most accurate volume calculations. A reference plane height reflecting the lake level was then set for each volume calculation depending on which contour was being used as the lake level. This method takes into account the underlying topography and yields an approximate volume for the lake, based on the conservative lake boundary reconstruction.

SUPPLEMENTAL REFERENCES

Adamiec, G., and Aitken, M. J., 1998, Dose-rate conversion factors: update: Ancient TL v. 16, no. 2, p. 37-50.

Balco, G., Briner, J., Finkel, R. C., Rayburn, J. A., Ridge, J. C., and Schaefer, J. M., 2009, Regional beryllium-10 production rate calibration for late-glacial northeastern North America: Quaternary Geochronology, v. 4, no. 2, p. 93-107.

Balco, G., Stone, J. O., Lifton, N. A., and Dunai, T. J., 2008, A complete and easily accessible means of calculating surface exposure ages or erosion rates from 10Be and 26Al measurements: Quaternary Geochronology, v. 3, no. 3, p. 174-195.

Barrows, T. T., Almond, P., Rose, R., Keith Fifield, L., Mills, S. C., and Tims, S. G., 2013, Late Pleistocene glacial stratigraphy of the Kumara-Moana region, West Coast of South Island, New Zealand: Quaternary Science Reviews, v. 74, no. 0, p. 139-159.

Barrows, T. T., Stone, J. O., Fifield, L. K., and Cresswell, R. G., 2001, Late Pleistocene Glaciation of the Kosciuszko Massif, Snowy Mountains, Australia: Quaternary Research, v. 55, no. 2, p. 179-189.

Bierman, P. R., and Caffee, M., 2002, Cosmogenic exposure and erosion history of Australian bedrock landforms: Geological Society of America Bulletin, v. 114, no. 7, p. 787-803.

Bøtter-Jensen, L., and Mejdahl, V., 1988, Assessment of beta dose-rate using a GM multicounter system: International Journal of Radiation Applications and Instrumentation. Part D. Nuclear Tracks and Radiation Measurements, v. 14, no. 1–2, p. 187-191.

Duller, G. A. T., 2003, Distinguishing quartz and feldspar in single grain luminescence measurements: Radiation Measurements, v. 37, no. 2, p. 161-165.

-, 2007, Assessing the error on equivalent dose estimates derived from single aliquot regenerative dose measurements: Ancient TL v. 25, p. 15-24.

Fenton, C. R., Hermanns, R. L., Blikra, L. H., Kubik, P. W., Bryant, C., Niedermann, S., Meixner, A., and Goethals, M. M., 2011, Regional 10Be production rate calibration for the past 12 ka deduced from the radiocarbon-dated Grøtlandsura and Russenes rock avalanches at 69° N, Norway: Quaternary Geochronology, v. 6, no. 5, p. 437-452.

Granger, D. E., and Smith, A. L., 2000, Dating buried sediments using radioactive decay and muogenic production of 26Al and 10Be: Nuclear Instruments and Methods in Physics Research Section B: Beam Interactions with Materials and Atoms, v. 172, no. 1-4, p. 822-826.

Grün, R., 2009, The “Age” programme for the calculation of luminescence age estimates: Ancient TL v. 27, p. 45-46.

Kaplan, M. R., Strelin, J. A., Schaefer, J. M., Denton, G. H., Finkel, R. C., Schwartz, R., Putnam, A. E., Vandergoes, M. J., Goehring, B. M., and Travis, S. G., 2011, In-situ cosmogenic ^{10}Be production rate at Lago Argentino, Patagonia: Implications for late-glacial climate chronology: Earth and Planetary Science Letters, v. 309, no. 1â€“2, p. 21-32.

Lifton, N. A., Bieber, J. W., Clem, J. M., Duldig, M. L., Evenson, P., Humble, J. E., and Pyle, R., 2005, Addressing solar modulation and long-term uncertainties in scaling secondary cosmic rays for in situ cosmogenic nuclide applications: Earth and Planetary Science Letters, v. 239, no. 1-2, p. 140-161.

Macklin, M. G., Woodward, J. C., Welsby, D. A., Duller, G. A. T., Williams, F. M., and Williams, M. A. J., 2013, Reach-scale river dynamics moderate the impact of rapid Holocene climate change on floodwater farming in the desert Nile: Geology, v. 41, no. 6, p. 695-698.

Murray, A. S., and Wintle, A. G., 2000, Luminescence dating of quartz using an improved single-aliquot regenerative-dose protocol: Radiation Measurements, v. 32, no. 1, p. 57-73.

Prescott, J. R., and Hutton, J. T., 1994, Cosmic ray contributions to dose rates for luminescence and ESR dating: Large depths and long-term time variations: Radiation Measurements, v. 23, no. 2–3, p. 497-500.

Putnam, A. E., Schaefer, J. M., Barrell, D. J. A., Vandergoes, M., Denton, G. H., Kaplan, M. R., Finkel, R. C., Schwartz, R., Goehring, B. M., and Kelley, S. E., 2010, In situ cosmogenic ^{10}Be production-rate calibration from the Southern Alps, New Zealand: Quaternary Geochronology, v. 5, no. 4, p. 392-409.

Stone, J. O., 2000, Air pressure and cosmogenic isotope production: Journal of Geophysical Research, v. 105, p. 23,753-723,759.

Williams, M. A. J., Adamson, D., Prescott, J. R., and Williams, F. M., 2003, New light on the age of the White Nile: Geology, v. 31, no. 11, p. 1001-1004.

Williams, M. A. J., Williams, F. M., Duller, G. A. T., Munro, R. N., El Tom, O. A. M., Barrows, T. T., Macklin, M., Woodward, J., Talbot, M. R., Haberlah, D., and Fluin, J., 2010, Late Quaternary floods and droughts in the Nile valley, Sudan: new evidence from optically stimulated luminescence and AMS radiocarbon dating: Quaternary Science Reviews, v. 29, no. 9-10, p. 1116-1137.

Table DR1. Site data

Sample	Longitude (°N)	Latitude (°E)	Altitude (m)	Horizon correction	Thickness/depth (cm)[1]	Muon production rate (atoms g^{-1} yr^{-1})
Jebel Hawaja						
JEB-01	12° 35' 3.3"	32° 50' 8.1"	426	1	3.0	0.210
JEB-02	12° 35' 3.6"	32° 50' 7.1"	427	1	2.5	0.210
JEB-03	12° 35' 4.0"	32° 50' 6.8"	425	1	3.0	0.210
Jebelein shoreline						
JEB-S06	12° 35' 7.5"	32° 49' 55.9"	402	1	2.5	0.209
JEB-S05	12° 35' 7.5"	32° 49' 55.9"		1	55	
JEB-S04	12° 35' 7.5"	32° 49' 55.9"		1	105	
JEB-S03	12° 35' 7.5"	32° 49' 55.9"		1	165	
JEB-S02	12° 35' 7.5"	32° 49' 55.9"		1	205	
JEB-S01	12° 35' 7.5"	32° 49' 55.9"		1	275	

1. Samples at Jebel Hawaja were exposed at the surface. Samples at the Jebelein shoreline are shown in depth below the surface (± 5 cm)

Table DR2. ^{10}Be results

Sample	Lab code	Production Rate (atoms g^{-1} yr^{-1}) Muons	$[^{10}Be]_c$ ($x10^5$ g^{-1})	Weathering rate (m/Ma)[1]
Jebel Hawaja				
JEB-01	ANU-M392-02		25.2 ± 1.70	0.73 ± 0.12
JEB-02	ANU-M392-03		9.90 ± 0.70	2.64 ± 0.33
JEB-03	ANU-M392-04		6.26 ± 0.46	4.62 ± 0.54
Section S2				
JEB-S2-06a	ANU-M392-05		5.01 ± 0.21	
JEB-S2-06b	ANU-M430-11		5.56 ± 0.26	
JEB-S2-05	ANU-M430-10		5.58 ± 0.24	
JEB-S2-04	ANU-M430-09		4.17 ± 0.18	
JEB-S2-03	ANU-M430-08		3.72 ± 0.18	
JEB-S2-02	ANU-M430-07		3.88 ± 0.18	
JEB-S2-01	ANU-M392-06		3.30 ± 0.14	

Data are normalised to NIST SRM 4325 assuming $^{10}Be/^{9}Be = 2.79 \times 10^{-11}$.
Carrier $^{10}Be/^{9}Be = <1 \times 10^{-15}$. ^{10}Be decay constant = 4.998×10^{-7} yr^{-1}.
Sample density for granite = 2.7 g cm^{-3}
1. Calculated using CRONUS online calculator and Wrapper script: 2.2, Main calculator: 2.1, Objective function: 2.0, Constants: 2.2.1, and Muons: 1.1 versions

Table DR3. Sample data, and concentrations of K, U and Th for luminescence samples

Site	Sample	Depth (m)	H_2O %	K (%)	U (ppm)	Th (ppm)
B	S11/1-1	1.20 ± 0.10	5 ± 2	1.10 ± 0.06	0.76 ± 0.04	2.59 ± 0.13
B	S11/1-2	1.50 ± 0.20	5 ± 2	1.09 ± 0.06	0.67 ± 0.03	2.00 ± 0.10
B	S11/1-3	2.35 ± 0.50	5 ± 2	0.97 ± 0.05	0.67 ± 0.03	1.82 ± 0.09
C	S10/5-2	1.10 ± 0.10	5 ± 2	0.87 ± 0.03	1.03 ± 0.07	3.72 ± 0.24
C	S10/5-3	1.50 ± 0.10	5 ± 2	0.90 ± 0.05	0.64 ± 0.03	1.78 ± 0.09
C	S10/5-4	1.65 ± 0.10	5 ± 2	0.92 ± 0.05	0.67 ± 0.03	1.33 ± 0.07
D	S11/3-1	0.80 ± 0.50	5 ± 2	0.93 ± 0.05	1.03 ± 0.05	1.14 ± 0.06
E	S11/WN1	0.00 ± 0.10	10 ± 5	0.97 ± 0.05	0.56 ± 0.03	0.78 ± 0.04

Table DR4. Dose rates, equivalent doses and ages for luminescence samples

Site	Sample	External β dose 'wet' (Gy/ka)	External γ dose 'wet' (Gy/ka)	Cosmic dose (Gy/ka)	Total dose rate (Gy/ka)	Aliquots accepted	Equivalent dose (Gy)	Age (ka)
B	S11/1-1	0.99 ± 0.04	0.45 ± 0.02	0.18 ± 0.02	1.62 ± 0.05	22	112 ± 6.2	69 ± 4
B	S11/1-2	0.90 ± 0.04	0.41 ± 0.02	0.17 ± 0.02	1.48 ± 0.04	23	130 ± 6.2	88 ± 5
B	S11/1-3	0.83 ± 0.04	0.38 ± 0.02	0.16 ± 0.04	1.36 ± 0.06	21	140 ± 10	103 ± 9
C	S10/5-2	0.79 ± 0.05	0.48 ± 0.05	0.19 ± 0.02	1.47 ± 0.04	22	15.3± 1.5	10.4 ± 1.1
C	S10/5-3	0.71 ± 0.03	0.36 ± 0.02	0.17 ± 0.02	1.24 ± 0.03	21	141 ± 9.6	113 ± 8
C	S10/5-4	0.85 ± 0.04	0.34 ± 0.01	0.17 ± 0.02	1.36 ± 0.04	24	156 ± 13	115 ± 10
D	S11/3-1	0.80 ± 0.03	0.38 ± 0.02	0.19 ± 0.04	1.36 ± 0.05	22	142 ± 7.0	104 ± 6
E	S11/WN1	0.65 ± 0.04	0.30 ± 0.02	0.30 ± 0.03	1.25 ± 0.06	24	0.00 ± 0.02	0.00 ± 0.02

Notes:

1) Grain Size 212-180 μm for all samples except S10/5-2 for which grains 125-180μm in diameter were used.
2) The recuperation for sample S11/WN1 was calculated as the percentage of the largest given dose rather than the natural signal which is near zero.

Figure DR1: Luminescence characteristics of a typical sample (S10/5-3). (a) Natural OSL decay curve. Note the log scale on the y-axis, (b) dose response curve and (c) radial plot showing the distribution of D_e values.

(a)

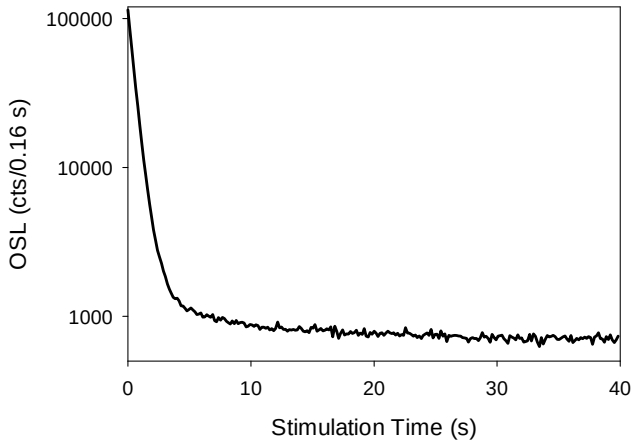

(b)

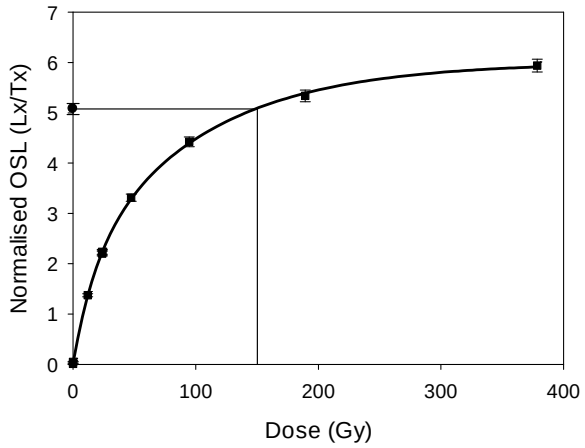

(c)

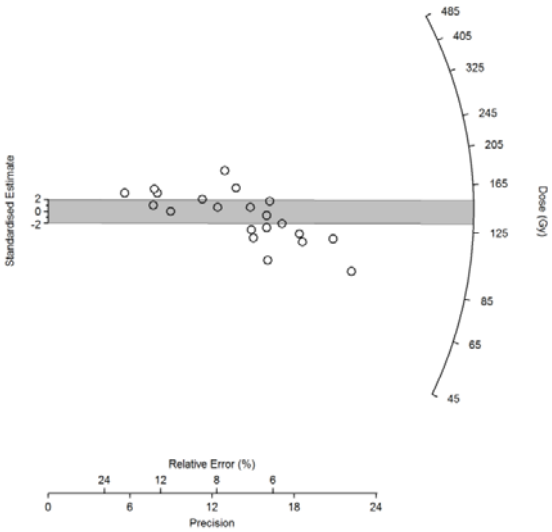
Standardised Estimate
2
0
-2
485
405
325
245
205
165
125
85
65
45
Dose (Gy)
Relative Error (%)
24
12
8
6
0
6
12
18
24
Precision